Journal of Materials Chemistry A

PAPER

View Article Online
View Journal | View Issue

Cite this: J. Mater. Chem. A, 2015, 3, 17312

Visible-light sensitive Cu(II)–TiO_2 with sustained anti-viral activity for efficient indoor environmental remediation†

Min Liu,[b] Kayano Sunada,[b] Kazuhito Hashimoto*[bc] and Masahiro Miyauchi*[ad]

Received 24th May 2015
Accepted 17th July 2015

DOI: 10.1039/c5ta03756e

www.rsc.org/MaterialsA

Visible-light sensitive photocatalysts are desirable for indoor environmental remediation applications. Photocatalysts used for indoor environmental applications must have efficient visible-light activity and sustainable function under dark conditions, as indoor light instruments are typically switched off during the night. Herein, we report the synthesis and optimization of a highly visible-light sensitive Cu(II)–TiO_2 nanocomposite with sustained anti-viral activity under dark conditions. The synthesized Cu(II)–TiO_2 exhibited superior volatile organic compound decomposition and anti-viral activity under visible-light irradiation. Its quantum efficiency for the decomposition of gaseous 2-propanol reached 68.7%. In addition, Cu(II)–TiO_2 completely inactivated the bacteriophage within 30 min of visible-light irradiation. Notably, the Cu(II)–TiO_2 photocatalyst also exhibited sustained anti-viral activity under dark conditions after visible-light irradiation treatment. Taken together, these findings indicate that the prepared Cu(II)–TiO_2 is potentially an effective risk-reduction material for indoor applications.

1. Introduction

Indoor air quality is an important health and safety factor due to its influence on population health and wellbeing.[1,2] The air levels of volatile organic compounds (VOCs) are of particular concern because these harmful chemicals cause a wide range of human health problems, including sick house syndrome.[3] Infectious pathogens are also frequently encountered in our daily environment and can adversely impact human health.[4,5] As a promising solution for environmental remediation, photocatalytic oxidation using semiconductors has attracted considerable attention. However, because most efficient photocatalysts are wide band-gap semiconductors, such as TiO_2, which are only activated by ultraviolet (UV) light irradiation, they have been limited to outdoor applications.[6–9] As indoor light sources contain low levels (below several $\mu W\ cm^{-2}$ in white light fluorescent light)[10] or no UV light (white incandescent light and white light emitting diodes [LEDs]), it is highly desirable to develop visible-light-sensitive photocatalysts for indoor environmental purification applications.

Over the past few decades, attempts to develop visible-light-sensitive photocatalysts have focused on the doping of TiO_2 with various transition metal ions or anions. Despite these efforts, most systems are not suitable for practical indoor applications because of their low quantum efficiencies (QEs) caused by the carrier recombination centers in metal-ion-doped TiO_2 or the low oxidation power and mobility of photogenerated holes in non-metal-doped TiO_2.[11–13] As an alternative strategy to doping, our group demonstrated that the surface modification of TiO_2 with Cu(II) or Fe(III) nanoclusters increases the visible-light-sensitivity of the resulting material without inducing impurity levels in the band gap.[14–19] In the case of Cu(II) nanocluster-grafted TiO_2 (Cu(II)–TiO_2), electrons in the valence band (VB) of TiO_2 are excited to the Cu(II) nanoclusters under visible-light irradiation through an interfacial charge transfer (IFCT) process. The introduction of excited electrons into the Cu(II) nanoclusters leads to the formation of Cu(I) species, which efficiently reduce oxygen molecules. During the IFCT process, holes with strong oxidative power for the decomposition of organic compounds are generated in the deep VB of TiO_2.[19] Thus, nanocluster-modified TiO_2 is a promising material for visible-light-sensitive photocatalytic applications.

Practical photocatalytic systems for indoor environmental remediation require the following characteristics: (i) composed of robust inorganic materials that are nontoxic and derived from naturally abundant elements; (ii) visible-light sensitivity with strong oxidation power; and (iii) anti-pathogenic (anti-bacterial and antiviral) effects, even under dark conditions.

[a]Department of Metallurgy and Ceramics Science, Graduate School of Science and Engineering, Tokyo Institute of Technology, 2-12-1 Ookayama, Meguro-ku, Tokyo 152-8552, Japan. E-mail: mmiyauchi@ceram.titech.ac.jp

[b]Research Center for Advanced Science and Technology, The University of Tokyo, 4-6-1 Komaba, Meguro-ku, Tokyo 153-8904, Japan. E-mail: hashimoto@light.t.u-tokyo.ac.jp

[c]Department of Applied Chemistry, School of Engineering, The University of Tokyo, 7-3-1 Hongo, Bunkyo-Ku, Tokyo 113-8656, Japan

[d]Japan Science and Technology Agency (JST), 4-1-8 Honcho Kawaguchi, Saitama 332-0012, Japan

† Electronic supplementary information (ESI) available: ICP, XPS, XRD, SEM, UV-Vis, photocatalytic performance measurements and calculated photocatalytic performances of Cu(II)–TiO_2 samples. See DOI: 10.1039/c5ta03756e

Cu(II) or Fe(III) nanocluster-grafted TiO_2 satisfy the first requirement, as they consist of non-toxic and earth-abundant elements.[20–22] Regarding visible-light sensitivity, the reaction rate and QE of Cu(II)-grafted TiO_2 are reportedly lower than those of Fe(III)-grafted TiO_2.[13–16] For the third requirement, copper oxides, particularly copper monoxide, are reported to have strong anti-viral activity, even under dark conditions,[20–23] as compared to iron-based oxides. Therefore, the optimization and improvement of Cu(II)–TiO_2, particularly with respect to increasing the visible-light activity and the sustained anti-viral function of Cu(II) nanocluster-modified TiO_2 are key challenges for developing efficient indoor applications for environmental remediation.

In this work, we comprehensively optimized the synthesis conditions for grafting Cu(II) nanoclusters onto TiO_2 to increase the reaction rate and QE of this photocatalyst. In addition to achieving the highest visible-light activity among the reported Cu(II)–TiO_2 photocatalysts, we demonstrated that Cu(II)–TiO_2 has sustained anti-viral activity, even under dark conditions after visible-light irradiation. Irradiation of Cu(II)–TiO_2 with visible light causes the Cu(I) species to reach an excited state, which is critical for the anti-viral function under both light and dark conditions. The Cu(II)–TiO_2 material is photocatalytically activated by indoor light irradiation and also maintains the anti-viral activity under dark conditions. Due to these properties, the presently synthesized Cu(II)–TiO_2 photocatalyst has great potential as an effective material for indoor purification applications aimed at minimizing risks to individual and public health.

2. Experimental section

2.1 Synthesis of Cu(II)–TiO_2 samples

Cu(II)–TiO_2 samples were prepared using a modified impregnation method, as described previously.[19] Briefly, commercial TiO_2 (MT-150A, Tayca Co.; rutile phase, 15 nm grain size) was annealed at 950 °C for 3 h. The calcined TiO_2 was treated with a 6 M HCl aqueous solution at 90 °C for 3 h under continuous stirring. After passing the reaction mixture through a membrane filter (0.025 μm, Millipore), the products were collected and then washed thoroughly with distilled water. The obtained TiO_2 powder was dried at 110 °C for 24 h and was then ground into a fine powder using an agate mortar and pestle. For the grafting of Cu(II) nanoclusters, 1 g TiO_2 powder was dispersed in 10 mL distilled water, to which copper chloride dihydrate ($CuCl_2 \cdot 2H_2O$, Wako, 99.9%) was then added. The weight fraction of Cu relative to TiO_2 was set to 0.1% and the pH value of the solution was adjusted to 12 using sodium hydroxide (NaOH). The resulting suspension was heated at 90 °C under continuous stirring for 1 h in a vial reactor. The obtained product was filtered through a 0.025 μm membrane filter (Millipore) and then washed with sufficient amounts of distilled water. Finally, the obtained product (denoted as Cu(II)–TiO_2 (950-HCl-12)) was dried at 110 °C for 24 h and was subsequently ground into a fine powder using an agate mortar and pestle. The above-mentioned procedure is the typical synthesis condition used to achieve the optimum photocatalytic activity of Cu(II)–TiO_2 and was determined by evaluating the following parameters: temperature of annealing on TiO_2 powder, aqueous HCl treatment to clean the TiO_2 surface, pH value for Cu(II) grafting, and amount of Cu(II) ions in aqueous solution.

2.2 Sample characterization

The crystal structures of the prepared Cu(II)–TiO_2 nanocomposites were measured by powder X-ray diffraction (XRD) at room temperature on a Rigaku D/MAX25000 diffractometer with a copper target ($\lambda = 1.54056$ Å). Elemental analyses of the samples were performed using an inductively coupled plasma-atomic emission spectrometer (ICPAES; P-4010, Hitachi). UV-visible absorption spectra were recorded by a diffuse reflection method using a UV-2550 spectrometer (Shimadzu). The morphologies of the prepared TiO_2 nanocomposites were investigated by scanning electron microscopy (SEM) using a Hitachi SU-8000 apparatus and transmission electron microscopy (TEM) using a Hitachi HF-2000 instrument with an acceleration voltage of 200 kV. The specific surface areas of the samples were determined from nitrogen absorption data at liquid nitrogen temperature using the Barrett–Emmett–Teller (BET) technique.[24] Briefly, the samples were degassed at 200 °C and the pressure was kept below 100 mTorr using a Micromeritics VacPrep 061 instrument for a minimum of 2 h prior to the analysis. Surface compositions were studied by X-ray photoelectron spectroscopy (XPS; model 5600, Perkin-Elmer). The binding energy data were calibrated with reference to the C 1s signal at 284.5 eV. The thermogravimetric analysis of the samples was performed using a Rigaku Thermo plus TG 8120 apparatus within a temperature range between 298 and 1473 K in air atmosphere and at a heating rate of 10 °C min^{-1}.

2.3 Evaluation of photocatalytic properties

The decomposition of gaseous (2-propanol) IPA in air atmosphere was chosen as a probe to evaluate the photocatalytic activities of the samples. For the analysis, 0.3 g powder samples were evenly dispersed on the bottom of a circular glass dish (5.5 cm^2), which was set in the center of a 500 mL cylindrical glass vessel reactor. After the vessel was sealed with a rubber O-ring and a quartz cover, the reactor was evacuated and filled with fresh synthetic air. To avoid organic contamination of the sample surface, the vessel was pre-illuminated with an Xe lamp (Luminar Ace 210, Hayashi Tokei Works) until the CO_2 generation rate was less than 0.02 μmol per day. The vessel was re-evacuated and re-filled with fresh synthetic air, and the internal pressure was maintained at approximately 1 atm. To begin the decomposition analysis, 300 ppm of gaseous IPA was injected into the vessel. Prior to light irradiation, the vessel was kept in the dark for a sufficient time (approximately 12 h) to achieve absorption/desorption equilibrium of IPA on the photocatalyst surface. The vessel was then irradiated by visible light with wavelengths from 420 to 530 nm emitted from an Xe lamp equipped with a combination of glass filters (B-47, L-42, and C-40C; AGC Techno Glass). The light intensity was measured using a spectroradiometer (USR-40D, Ushio) and was set to 1 mW cm^{-2}. During the light irradiation, 1 mL gaseous samples

were periodically extracted from the reaction vessel to detect the concentrations of IPA, acetone and CO_2 using a gas chromatograph (model GC-8A, Shimadzu Co., Ltd).

2.4 Evaluation of anti-viral activity

Cu(II)–TiO_2 was coated on a glass substrate (2.5 cm × 2.5 cm) by simply drop casting 150 μL of an ethanol suspension of Cu(II)–TiO_2 (1 mg mL^{-1}). The total amount of Cu(II)–TiO_2 coated on the substrate was 0.3 mg/6.25 cm^2, which is equal to 0.48 g m^{-2}. The glass surface was dried and then sterilized at 120 °C for 3 h. *Qβ* bacteriophage (NBRC 20012) and *Escherichia coli* (NBRC 13965) as the host bacterium were used in the evaluation experiment. A stock suspension of *Qβ* bacteriophage (~1.2 × 10^{11} plaque forming units per mL [PFUs mL^{-1}]) was used to infect *E. coli* cells at 35 °C for 10 min, and then was plated onto a double-layered medium, which was prepared with Nutrient Broth (Difco) and agar (Difco) by adjusting the agar concentration of the bottom layer to 1.5% and that of the top layer to 0.5%. The plates were then further incubated overnight at 35 °C, and the top agar layer containing the cells and bacteriophage was then collected and added to 2 mL per plate SM buffer (0.1 M NaCl, 8 mM $MgSO_4$, 50 mM Tris–HCl [pH 7.5] and 0.1% gelatin) at 4 °C overnight. The solution was centrifuged (8000×*g*, 4 °C, 20 min) and the resulting supernatant containing the bacteriophage was collected and filtered (0.22 μm, Millipore, MA). The bacteriophage solution was diluted with PBS to give approximately 2.5 × 10^9 PFUs mL^{-1} and 50 μL of the diluted suspension was then pipetted onto the Cu(II)–TiO_2 coated glass. The glass samples were irradiated using 10 W white light bulbs at an illuminance of 1000 lux. The light illuminance was measured using an illuminance meter (IM-5, Topcon), and irradiation with visible light with wavelengths above 400 nm was performed using a white fluorescence light bulb through a UV cutoff film. After irradiation, the bacteriophage suspension was collected into SM buffer (10 mL). An appropriate dilution of the collected suspension was used to infect *E. coli* cells, which were then plated onto nutrient agar medium using the above-described double-layer method to determine the number of plaques.

3. Results and discussion

3.1 Improvement of visible-light sensitivity of Cu(II)–TiO_2

To improve the visible-light activity of Cu(II)–TiO_2, we investigated the effect of the synthesis conditions, including the pre-annealing treatment of bare TiO_2 powder, washing treatment of TiO_2 under aqueous acid conditions, pH during the grafting of Cu(II) nanoclusters, and the amount of Cu(II) nanoclusters, on the photocatalytic activity. To investigate the effect of the pre-annealing conditions for TiO_2 powder, XRD patterns of TiO_2 powder annealed for 3 h at temperatures ranging from 300 to 1150 °C were recorded (Fig. 1a). TG-DTA analysis was also performed and revealed that endothermic and exothermic peaks of the TiO_2 powder appeared at approximately 440 and 935 °C, respectively (ESI, Fig. S1†). The endothermic peak mainly originated from the removal of surface-absorbed compounds,[25] which resulted in a decrease of the powder weight between 400 and 500 °C. The exothermic peak was attributed to the crystallization of the powder,[25] indicating that the TiO_2 powder obtained at approximately 935 °C possessed good crystallinity. The XRD patterns of the annealed powders showed that all of the samples had a rutile structure (JCPDS card no. 21-1276). In addition, the diffraction peaks became sharper with increasing annealing temperature, indicating that the crystallinity of the samples was improved by the annealing treatment. Fig. 1b shows the influence of the pre-annealing temperature on the specific surface area and crystallite size of TiO_2, as determined by Scherrer's equation.[26] The annealing treatment resulted in an increase in the crystallite size of the TiO_2 powder (from ~15 to ~125 nm), but markedly decreased the total surface area. SEM image analysis clearly showed that the particle size increased with increasing annealing temperature (Fig. S2†). Notably, performing the annealing step at over 950 °C resulted in significant crystal growth and caused the color of the powder to change from white to brown (Fig. S3†), indicating the introduction of oxygen defects or generation of Ti^{3+} species into the sample.[17] Oxygen defects or Ti^{3+} species have been demonstrated to reduce the photocatalytic performance of TiO_2.[17] Furthermore, the surface areas of the samples obtained at 950 and 1150 °C were ~5.8 and ~1.2 m^2 g^{-1}, respectively, which are markedly smaller than the ~110 m^2 g^{-1} area of the starting TiO_2 powders.

Fig. 2 shows the TEM and energy-dispersive X-ray spectroscopy (EDS) analyses of the Cu(II)–TiO_2 (950-HCl-12) sample, which was prepared by pre-annealing TiO_2 at 950 °C, acid treating before Cu(II) grafting, and grafting the Cu(II) clusters under pH 12 conditions. These conditions were determined to result in optimal photocatalytic activity of the prepared material, as described in detail below. The TEM analysis revealed that Cu(II) nanoclusters were well dispersed on the surface of TiO_2 (Fig. 2a). High-resolution TEM (HRTEM) image analysis showed that the Cu(II) nanoclusters were ~3 nm in size and well attached to the TiO_2 surface (Fig. 2b). EDS point analysis (Fig. 2c) revealed that the nanoclusters were composed of Cu. We also measured the XPS spectra of the Cu(II)–TiO_2 (950-HCl-12) sample (Fig. S4†) and confirmed that Cu(II) species were present on the TiO_2 surface. The optical absorption properties of Cu(II)–TiO_2 and bare TiO_2 were recorded and are shown in the ESI (Fig. S5†). For bare TiO_2, no absorption was observed in the UV-vis spectra at wavelengths shorter than

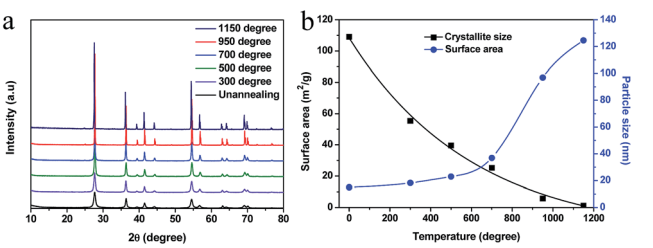

Fig. 1 (a) XRD patterns of TiO_2 samples obtained at various annealing temperatures and (b) crystallite sizes and surface areas of TiO_2 *versus* annealing temperature.

420 nm other than the band-gap excitation of rutile TiO_2. However, after the grafting of Cu(II) nanoclusters on the TiO_2 surface, new absorptions in the regions of 420–550 and 700–800 nm were observed (Fig. S5†). The slight increase in absorption in the former region was attributed to the IFCT process of VB electrons to surface Cu(II) nanoclusters, whereas the increase in the latter region was assigned to a simple d–d transition of Cu(II).[14]

The photocatalytic activity of the Cu(II)–TiO_2 samples was evaluated by the visible-light-induced oxidation of IPA, which is frequently used as a representative gaseous VOC and is a harmful indoor air pollutant.[27] The photocatalytic oxidative decomposition of IPA proceeds *via* the formation of acetone as an intermediate, followed by the further decomposition of acetone to the final products, CO_2 and H_2O (Fig. 3a).[28] During the photocatalytic tests, the light intensity was adjusted to ~1 mW cm^{-2}, which corresponds to an illuminance of ~300 lux and is comparable to the intensity of typical indoor fluorescent and LED light. The wavelength of the irradiation light ranged from 420 to 530 nm, and the initial IPA concentration was set to 300 ppmv (~6 μmol). For all samples shown in Fig. 3, Cu(II) nanoclusters were grafted at pH 7. The photocatalytic performance of the TiO_2 samples increased with increasing annealing temperature up to 950 °C (Fig. 3b). The performance of the TiO_2 sample obtained at an annealing temperature of 950 °C was markedly higher than that of the un-annealed sample. The QE was determined by the reaction rate (R) and number of absorbed photons (Fig. S6†). For the sample prepared by pre-annealing treatment at 950 °C, the QE was 13.2%. However, when the annealing temperature exceeded 950 °C, the photocatalytic activity of the samples markedly decreased. These results are attributable to the formation of oxygen or Ti^{3+} defects at high temperature. Thus, the sample obtained at 1150 °C exhibited the lowest photocatalytic performance. This finding indicates that TiO_2 with good crystallinity and few defects, meaning less recombination centers, is important for the photocatalytic activity of the Cu(II)–TiO_2 system, even though the TiO_2 surface area is significantly decreased. In addition to crystallinity, aqueous acid treatment of the TiO_2 powder prior to the grafting of Cu(II) clusters is critical for the removal of surface contaminants and achieving high photocatalytic performance. Previous studies have reported that the presence of contaminants, such as alkali and alkaline earth elements (Na^+ or Ca^{2+}), markedly deteriorates the photocatalytic activity of TiO_2.[29,30] The present XPS spectra analysis revealed that surface contaminants, including Na^+ and Ca^{2+}, were removed by acid treatment in hydrochloric acid (HCl) solution (Fig. S7†). Owing to the high acid stability of TiO_2, no obvious difference could be observed in the morphologies of the TiO_2 samples with or without acid treatment (Fig. S8†). Thus, the QE value of Cu(II)–TiO_2 was improved from 13.2% to 30.3% by acid treatment (950-HCl-7 in Table 1), since the surface contaminant was removed by acid treatment, resulting in efficient charge transfer between TiO_2 and Cu(II) clusters.

In the above experiment, Cu(II) grafting was performed under neutral pH conditions. To examine the effect of pH during grafting on the photocatalytic activity of Cu(II)–TiO_2, we next attempted to optimize the pH of the solution used for the grafting of Cu(II) nanoclusters. We used the TiO_2 powder prepared using a pre-annealing temperature of 950 °C and HCl treatment as a starting material. From the UV-Vis spectra of the Cu(II)–TiO_2 samples prepared at different pH values, it can be seen that visible-light absorption caused by either the IFCT process or the d–d transition of Cu(II) increased with increasing alkalinity (Fig. 4a). The increase of the d–d transition of Cu(II) indicates that the amount of Cu(II) had increased in the samples prepared at higher pH, a finding that was confirmed by XPS and ICP measurements (Fig. S9 and Table S1†). At pH values below 12, only a limited amount of Cu(II) nanoclusters (less than 20% of added $CuCl_2$ salt in aqueous solution) was grafted on the TiO_2 surface. In contrast, when the pH value was above 12, nearly all Cu(II) ions in solution were grafted onto the TiO_2 surface as nanoclusters. Thus, the IFCT visible-light absorption sharply increased at pH values over 12 (Fig. 4a, inset). The observed influence of the pH on the amount of grafted Cu(II) nanoclusters may be due to the dependence of the surface charge of TiO_2 on pH. Under strong acidic (HCl) conditions, the

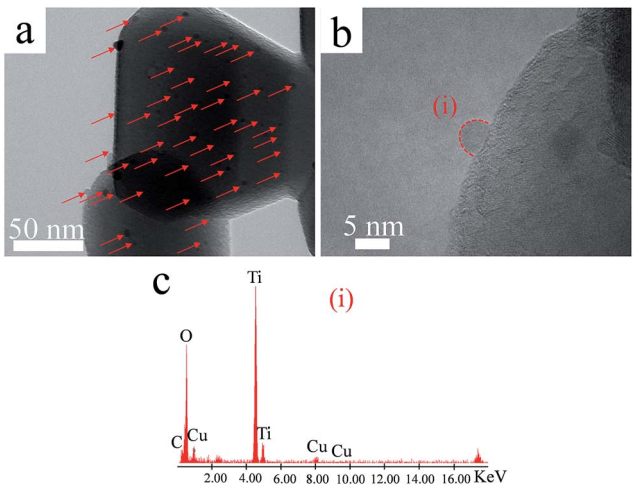

Fig. 2 (a) TEM and (b) HRTEM images of Cu(II)–TiO_2 (950-HCl-12). Nanoclusters (indicated by red arrows) were highly dispersed on the TiO_2 surface. In (b), the short dashed curve outlines a single Cu(II) nanocluster. The good attachment of nanoclusters and TiO_2 can be clearly observed. (c) EDS point analysis of the Cu(II) nanocluster on the point (i) in panel (b).

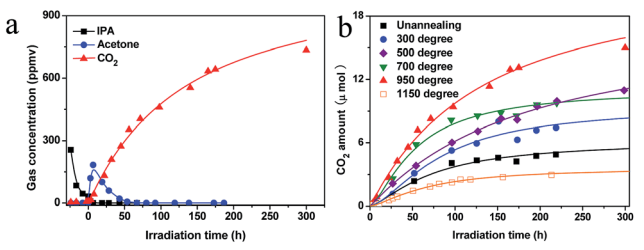

Fig. 3 (a) Representative time-dependent gas concentrations during IPA decomposition by the Cu(II)–TiO_2 (950-7) sample under visible-light irradiation. (b) Comparative analysis of CO_2 generation by Cu(II)–TiO_2 synthesized at different temperatures under the same conditions.

Table 1 Summary of the photocatalytic performances of the Cu(II)–TiO_2 samples under different experimental conditions

Experimental conditions	pH	Cu(II) amount	Initial photons (quanta s^{-1} cm^{-2})	Absorbed photons (quanta sec^{-1} cm^{-2})	Reaction rate (μmol h^{-1})	QE (%)
pH dependence	2	0.1%	1.3×10^{16}	4.43×10^{14}	0.07	15.8
	4	0.1%	1.3×10^{16}	4.53×10^{14}	0.10	22.1
	7	0.1%	1.3×10^{16}	4.62×10^{14}	0.14	30.3
	10	0.1%	1.3×10^{16}	4.84×10^{14}	0.24	49.6
	12	0.1%	1.3×10^{16}	5.82×10^{14}	0.40	68.7
	14	0.1%	1.3×10^{16}	6.48×10^{14}	0.05	7.7
Cu(II) amount dependence	12	0.05%	1.3×10^{16}	4.98×10^{14}	0.32	64.2
	12	0.25%	1.3×10^{16}	7.94×10^{14}	0.33	41.6
	12	0.5%	1.3×10^{16}	9.55×10^{14}	0.13	13.6

TiO_2 surface is positively charged, as the pH value of the isoelectric point of bare TiO_2 is neutral at a pH of approximately 6.[31] Therefore, high pH conditions cause a negative shift in the surface TiO_2 charge, allowing for the efficient grafting of Cu(II) clusters. It is noted that we could not see the obvious loading amount dependence on photocatalytic activities, when the pH condition was neutral (Fig. S10†). These results also imply that the TiO_2 surface is positively charged after the acid treatment, and that the amount of loaded Cu(II) nanoclusters strongly depends on the pH of the solution. It is also possible that the dependence of the Cu(II) nanocluster grafting efficiency on pH is due to the hydrolysis of Cu(II) ions. Cu(II) ions are poorly soluble in highly alkaline solutions and precipitate as black-brownish CuO particles, as shown in Fig. S11.† In the present study, when the pH value of Cu(II) solution was increased to 14, we confirmed that CuO crystals were formed (Fig. S12†). Our group previously demonstrated that bulk crystal CuO particles poorly consume photogenerated electrons,[19] which is crucial for the IFCT process and the multi-electron reduction reaction. At pH values below 12, the heterogeneous hydrolysis of Cu(II) ions occurs on the surface of TiO_2 powder, resulting in a good junction between the Cu(II) nanoclusters and TiO_2 surface. Under the present experimental conditions, a pH value of 12 was optimal for the grafting of Cu(II) nanoclusters. Further, XPS spectra showed that the chemical states of elemental Ti and O were similar to those of Cu(II)–TiO_2 prepared at pH 12 and bare TiO_2 (Fig. S13†). Taken together, the results indicate that the chemical state and environment surrounding the Cu(II) nanoclusters in the Cu(II)–TiO_2 sample prepared at pH 12 were highly similar to those of a previously characterized Cu(II)–TiO_2 system.[14,19]

Fig. 4b shows the photocatalytic performances of the Cu(II)–TiO_2 (950-HCl) samples prepared at different pH values. It can be seen that the photocatalytic activity of Cu(II)–TiO_2 increased with increasing pH during the grafting of Cu(II) nanoclusters. The limited photocatalytic performance of the samples prepared at pH values less than 12 is likely attributable to the limited amount of Cu(II) nanoclusters on the positively charged TiO_2 surface. As the pH increased, the TiO_2 surface became more negative, and the amount of surface-grafted Cu(II) nanoclusters increased, leading to a corresponding increase in the photocatalytic activity of Cu(II)–TiO_2. Notably, the sample exhibited the highest performance at a pH of 12. The calculated QE and R for this sample were 68.7% and 0.40 μmol h^{-1}, respectively (Table 1), which have been the highest values reported to date for a Cu(II)–TiO_2 photocatalytic system.[14,17,19,21,22] A further increase in the pH value resulted in a drastic decrease of the photocatalytic performance, because the Cu(II) nanoclusters were changed into CuO crystals, leading to a marked decrease in the multi-electron reduction reaction rate and the reduced consumption of photogenerated electrons.[19]

We also attempted to optimize the amount of Cu(II) grafted on the TiO_2 surface at pH 12 (Fig. 5). ICP measurements showed that nearly all of the Cu(II) was grafted on the surface of TiO_2 at pH 12 and that the total amount of grafted Cu(II) increased with increasing levels of the initial Cu(II) concentration (Table S2†). Consistent with this finding, the visible-light absorption of the Cu(II)–TiO_2 samples increased with increasing amounts of grafted Cu(II) (Fig. 5a). Measurements of the photocatalytic performances of the Cu(II)–TiO_2 samples showed that their visible-light activities were first increased with increasing amounts of Cu(II). When the amount of Cu(II) exceeded 0.1%, the photocatalytic activity of Cu(II)–TiO_2 decreased. The results demonstrated that 0.1% is the optimal amount of grafted Cu(II) nanoclusters for Cu(II)–TiO_2. Notably, the photocatalytic activity of Cu(II)–TiO_2 prepared under these conditions was markedly superior to that of $TiO_{2-x}N_x$, which is considered to be one of the most efficient visible-light photocatalyts.[32] The calculated QE of the $TiO_{2-x}N_x$ samples was only 3.9%, which is dramatically lower than that of our Cu(II)–TiO_2 (950-HCl-12) sample of 68.7% (Table 1).

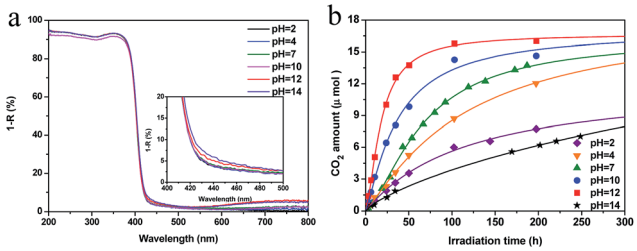

Fig. 4 (a) UV-Vis spectra for Cu(II)–TiO_2 (950-HCl) samples prepared at different pH values. (b) CO_2 generation curves for the prepared samples under visible-light irradiation.

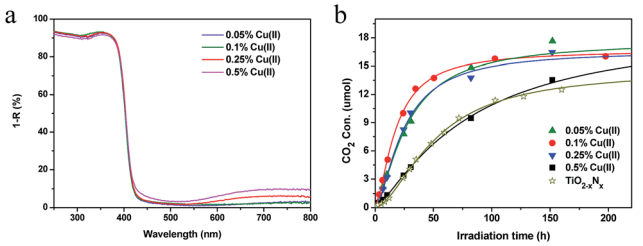

Fig. 5 (a) UV-Vis spectra for Cu(II)–TiO_2 samples with different amounts of grafted Cu(II) at pH 12 and (b) photocatalytic activities of the Cu(II)–TiO_2 samples in (a) and N-doped TiO_2 under visible-light irradiation.

3.2 Anti-viral activity of Cu(II)–TiO_2

In addition to the photocatalytic properties of TiO_2, the anti-bacterial and anti-viral properties of TiO_2 under light irradiation are also important for its practical applications.[33–35] The photocatalytic inactivation of pathogenic microorganisms by Cu(II)–TiO_2 was evaluated using thin film samples that were prepared by coating suspensions of Cu(II)–TiO_2 (950-HCl-12) on glass substrates. Bacteriophage *Qβ* was used as a model virus to measure the anti-viral activity of Cu(II)–TiO_2.[23] The anti-viral activity of the Cu(II)–TiO_2 nanocomposite was tested by the plaque assay according to the standard evaluation procedure for the photocatalytic antiviral effect (Japanese Industrial Standards, JIS R1756). In the assay, test solutions containing bacteriophage *Qβ* were used to infect *E. coli* (NBRC 13965), and the bacteriophage *Qβ* concentration was determined from the number of PFUs mL^{-1}.

As can be seen in Fig. 6a, the Cu(II)–TiO_2 (950-HCl-7) sample exhibited only a negligible degree of bacteriophage inactivation in the dark, whereas obvious inactivation was observed under visible-light irradiation. Specifically, viral inactivation reached 99% and 99.99% under visible-light irradiation for 1 and 2 h, respectively. Notably, the Cu(II)–TiO_2 (950-HCl-12) displayed a $\log_{10}(6.5)$ reduction of bacteriophage after only 30 min of visible-light irradiation (Fig. 6b). This bacteriophage inactivation performance was identical to that of our previously reported Cu_xO/TiO_2 samples.[20] Fig. 6c shows the effect of pre-irradiation treatment on the anti-viral activity of the Cu(II)–TiO_2 (950-HCl-12) sample under dark conditions. After 1 h of visible light pre-irradiation treatment, followed by 1 h incubation under dark conditions, 99.9% of viral particles were inactivated. The anti-viral performance of Cu(II)–TiO_2 (950-HCl-12) under dark conditions was superior to that of Cu(II)–TiO_2 (950-HCl-7, Fig. 6a) and conventional Cu(II)–TiO_2 (950-7) samples under visible-light irradiation,[20] as only two orders (99%) of virus were inactivated by the Cu(II)–TiO_2 samples during visible-light irradiation for 1 h. As shown in Fig. 6b, the Cu(II)–TiO_2 (950-HCl-12) sample only exhibited low anti-viral activity under dark conditions without irradiation treatment, confirming that the anti-viral activity of this photocatalytic material in the dark was attributable to the pre-irradiation treatment. Furthermore, the anti-viral activity was directly influenced by the intensity of the light used for the pre-irradiation treatment. The sustained anti-viral activity of Cu(II)–TiO_2 (950-HCl-12) was enhanced when strong visible-light sources, such as a fluorescent lamp, or UV light sources, such as a black light bulb, were used for the irradiation treatment (Fig. S14†).

The anti-bacterial and anti-viral properties of TiO_2 under light irradiation have been widely investigated[33,34] and are attributed to the direct oxidation of virus by photogenerated holes or reactive radical species, such as $^{\bullet}OH$ radical, O_2^-, and H_2O_2.[35] However, the inactivation speed of bacteria and virus on TiO_2 was limited by the step of disordering the outer membranes of bacteria and virus.[33] The anti-viral effects of Cu metal, Cu oxides, and Cu(II) ions have also been determined.[23,36] The anti-viral effects on Cu species are attributed to the blocking of functional groups of proteins and inactivation of enzymes.[23] Our recent study demonstrated that Cu(I) species in Cu nanoclusters are much more effective than Cu metals or Cu(II) species for enhancing the anti-viral and anti-bacterial effects of TiO_2 photocatalysts.[20] Irie *et al.*[19] investigated the role of Cu(II) nanoclusters in electron-trapping by *in situ* X-ray absorption fine structure (XAFS) analysis under visible-light irradiation in the presence of IPA and absence of oxygen and found that Cu(I) was generated under these conditions. Therefore, the presently observed anti-viral activity of Cu(II)–TiO_2 (950-HCl-12) under dark conditions after visible-light irradiation was induced by the Cu(I) species in the solid-state Cu(II) nanoclusters. Previous studies have demonstrated that the combination of TiO_2 with CuO or Cu_2O resulted in visible-light absorption and electron trapping among TiO_2 and these copper oxides under visible-light irradiation.[37,38] The trapped electrons lead to the formation of highly reduced states of TiO_2/Cu(I) species, which are highly stable, even under oxygen-saturated conditions, at the interface between TiO_2 and Cu(II) species.[39–41]

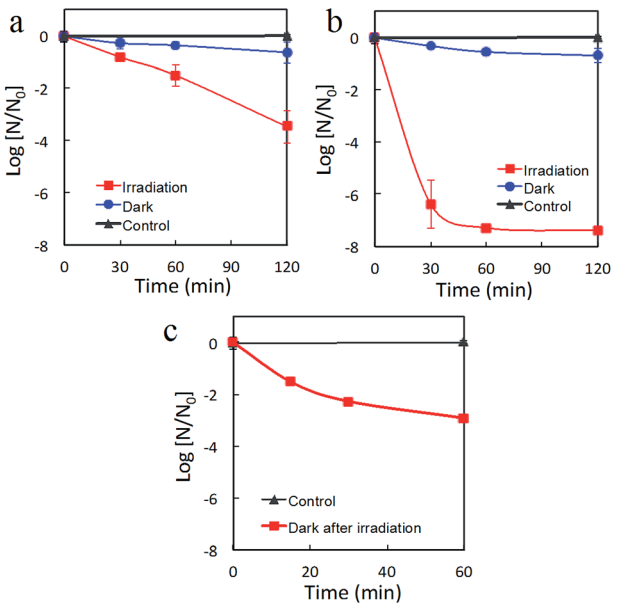

Fig. 6 Inactivation of *Qβ* bacteriophage by (a) Cu(II)–TiO_2 (950-HCl-7) and (b) Cu(II)–TiO_2 (950-HCl-12) under dark conditions and visible-light irradiation, and by (c) Cu(II)–TiO_2 (950-HCl-12) under dark conditions after pre-irradiation treatment with visible-light.

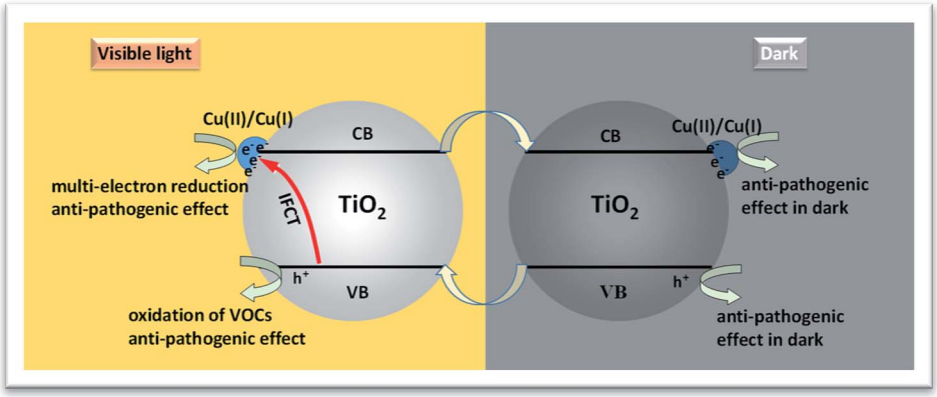

Fig. 7 Proposed processes of photocatalysis and inactivation of viruses and bacteria under visible-light irradiation and dark conditions.

The photogenerated electrons are trapped and stored in metal oxide semiconductors as donors and are gradually oxidized under air under dark conditions.[37–41]

Fig. 7 shows the possible mechanism underlying the sustained anti-viral activity of our photocatalyst in the absence of light irradiation. Under visible-light irradiation, electrons in the VB of TiO_2 are excited to the surface Cu(II) nanoclusters in a process that represents a form of IFCT and results in the transformation of Cu(II) into Cu(I), with holes remaining in the VB. The generated Cu(I) can efficiently reduce oxygen molecules *via* a multi-electron reduction process that regenerates Cu(II).[14–16] The holes generated in the VB of TiO_2 possess strong oxidation power to decompose VOCs, a property that explains the high photooxidation activity of the TiO_2 (950-HCl-12) nanocomposites for IPA decomposition under visible-light irradiation. In addition, it has been demonstrated that Cu(I) species are very effective for enhancing the anti-viral and anti-bacterial effects of TiO_2 photocatalysts even under dark conditions.[20] Following irradiation with visible light, holes generated in the VB of TiO_2, in combination with Cu(I) species, can also attack the outer membrane, proteins, and nucleic acid (DNA and RNA) of viruses and bacteria, resulting in their death and inactivation.[20] Therefore, the obtained TiO_2 (950-HCl-12) nanocomposites exhibited a marked activity for anti-bacteria and antivirus under visible light irradiation. For the sustainability of antivirus activity under dark conditions, the remaining Cu(I) species play an important role. It has been reported that the combination of TiO_2 with copper oxides, such as CuO or Cu_2O, not only resulted in visible-light absorption but also electron trapping at the interfaces among TiO_2 and these copper oxides under visible-light irradiation.[37,38] Trapped electrons in Cu^{2+} species as Cu^{1+} states are thermodynamically more stable than those in the conduction band (CB) of TiO_2,[37,38] since the redox potential of Cu^{2+}/Cu^{+} in the Cu(II) nanoclusters is more positive than that in the CB of TiO_2. Thus, a part of electrons could be trapped in Cu(II) nanoclusters near the interfaces, resulting in the prevention of recombination with holes in the VB.[42] These trapped electrons in Cu(II) nanoclusters as Cu^{1+} species contribute to the sustained anti-bacterial and anti-viral properties under dark conditions. Moreover, the photocatalytic activity of the TiO_2 (950-HCl-12) sample was stable in air with a turnover number of greater than 60. These results indicate that both the photocatalytic VOC decomposition and anti-pathogenic effects of our synthesized Cu(II)–TiO_2 (950-HCl-12) nanocomposites can be sustained for long-term operation in indoor environments. These properties suggest that Cu(II)–TiO_2 (950-HCl-12) is a promising material for indoor environmental risk-reduction applications.

4. Conclusion

In summary, we succeeded in preparing highly visible-light-active Cu(II)–TiO_2 nanocomposites with sustained anti-viral properties through comprehensive optimization of the synthesis conditions, such as pre-annealing treatment of bare TiO_2 powder, washing treatment of TiO_2 under aqueous acid conditions, and the pH value of the solution and the amount of grafted Cu(II) nanoclusters. By optimizing the crystallinity, the interfacial junction between TiO_2 and Cu(II) nanoclusters, and the amount of Cu(II) nanoclusters, the synthesized Cu(II)–TiO_2 nanocomposites exhibited efficient IFCT and reductive energy storage properties. Thus, the photocatalytic nanocomposites efficiently decomposed VOCs and had strong anti-pathogenic effects under indoor conditions. Notably, the nanocomposites displayed sustained anti-viral activity under dark conditions after light irradiation. Based on these properties, our Cu(II)–TiO_2 nanocomposites are promising materials for risk-reduction applications in indoor environments. In addition, the synthesis approach described here represents a fundamental route to develop efficient nanocomposites for numerous target applications.

Acknowledgements

This work was performed under the management of the Project to Create Photocatalysts Industry for Recycling-Oriented Society supported by the New Energy and Industrial Technology Development Organization (NEDO) in Japan. This research was also supported by the ACT-C program of the Japan Science and Technology (JST) Agency.

References

1 J. D. Spengler and K. Sexton, *Science*, 1983, **221**, 9–17.
2 N. E. Klepeis, W. C. Nelson, W. R. Ott, J. P. Robinson, A. M. Tsang, P. Switzer, J. V. Behar, S. C. Hern and W. H. Engelmann, *J. Exposure Anal. Environ. Epidemiol.*, 2001, **11**, 231–252.
3 K. Harada, A. Hasegawa, C. N. Wei, K. Minamoto, Y. N. Noguchi, K. Hara, O. Matsushita, K. Noda and A. Ueda, *J. Health Sci.*, 2010, **56**, 488–501.
4 D. M. Morens, G. K. Folkers and A. S. Fauci, *Nature*, 2004, **430**, 242–249.
5 K. E. Jones, N. G. Patel, M. A. Levy, A. Storeygard, D. Balk, J. L. Gittleman and P. Daszak, *Nature*, 2008, **451**, 990–993.
6 A. Fujishima, X. Zhang and A. D. Tryk, *Surf. Sci. Rep.*, 2008, **63**, 515–582.
7 M. R. Hoffmann, S. T. Martin, W. Choi and D. W. Bahnemann, *Chem. Rev.*, 1995, **95**, 69–96.
8 A. L. Linsebigler, G. Q. Lu and J. T. Yates, *Chem. Rev.*, 1995, **95**, 735–758.
9 K. Hashimoto, H. Irie and A. Fujishima, *Jpn. J. Appl. Phys.*, 2005, **44**, 8269–8285.
10 M. Miyauchi, A. Nakajima, K. Hashimoto and T. Watanabe, *Adv. Mater.*, 2000, **12**, 1923–1927.
11 W. Y. Choi, A. Termin and M. R. Hoffmann, *J. Phys. Chem.*, 1994, **98**, 13669–13679.
12 P. V. Kamat and D. Meisel, *Curr. Opin. Colloid Interface Sci.*, 2002, **7**, 282–287.
13 H. Irie, Y. Watanabe and K. Hashimoto, *J. Phys. Chem. B*, 2003, **107**, 5483–5486.
14 H. Irie, S. Miura, K. Kamiya and K. Hashimoto, *Chem. Phys. Lett.*, 2008, **457**, 202–205.
15 H. G. Yu, H. Irie and K. Hashimoto, *J. Am. Chem. Soc.*, 2010, **132**, 6898–6899.
16 H. G. Yu, H. Irie, Y. Shimodaira, Y. Hosogi, Y. Kuroda, M. Miyauchi and K. Hashimoto, *J. Phys. Chem. C*, 2010, **114**, 16481–16487.
17 M. Liu, X. Q. Qiu, M. Miyauchi and K. Hashimoto, *Chem. Mater.*, 2011, **23**, 5282–5286.
18 M. Liu, X. Q. Qiu, M. Miyauchi and K. Hashimoto, *J. Am. Chem. Soc.*, 2013, **135**, 10064–10072.
19 H. Irie, K. Kamiya, T. Shibanuma, S. Miura, D. A. Trky, T. Yokoyama and K. Hashimoto, *J. Phys. Chem. C*, 2009, **113**, 10761–10766.
20 X. Q. Qiu, M. Miyauchi, K. Sunada, M. Minoshima, M. Liu, Y. Lu, D. Li, Y. Shimodaira, Y. Hosogi, Y. Kuroda and K. Hashimoto, *ACS Nano*, 2012, **6**, 1609–1618.
21 M. Liu, X. Q. Qiu, M. Miyauchi and K. Hashimoto, *J. Mater. Chem. A*, 2014, **2**, 13571–13579.
22 M. Liu, R. Inde, M. Nishikawa, X. Q. Qiu, D. Atarashi, E. Sakai, Y. Nosaka, K. Hashimoto and M. Miyauchi, *ACS Nano*, 2014, **8**, 7229–7238.
23 K. Sunada, M. Minoshima and K. Hashimoto, *J. Hazard. Mater.*, 2012, **235–236**, 265–270.
24 S. Brunauer, P. H. Emmett and E. Teller, *J. Am. Chem. Soc.*, 1938, **60**, 309–319.
25 A. S. Attar, M. S. Ghamsari, F. Hajiesmaeilbaigi, S. Mirdamadi, K. Katagiri and K. Koumoto, *J. Mater. Sci.*, 2008, **43**, 5924–5929.
26 B. D. Cullity and S. R. Stock, *Elements of X-Ray Diffraction*, Prentice-Hall Inc., Upper Saddle River, NJ, 3rd edn, 2001.
27 P. Wolkoff and G. D. Nielsen, *Atmos. Environ.*, 2001, **35**, 4407–4417.
28 Y. Ohko, K. Hashimoto and A. Fujishima, *J. Phys. Chem. A*, 1997, **101**, 8057–8062.
29 H. G. Yu, J. G. Yu and B. Cheng, *Catal. Commun.*, 2006, **7**, 1000–1004.
30 J. G. Yu and X. J. Zhao, *Mater. Res. Bull.*, 2000, **35**, 1293–1301.
31 F. Boccuzzi, A. Chiorino, G. Martra, M. Gargano, N. Ravasio and B. Carrozzini, *J. Catal.*, 1997, **165**, 129–139.
32 R. Asahi, T. Morikawa, T. Ohwaki, K. Aoki and Y. Taga, *Science*, 2001, **293**, 269–271.
33 M. Cho, H. M. Chung, W. Y. Choi and J. Y. Yoon, *Appl. Environ. Microbiol.*, 2005, **71**, 270–275.
34 K. Sunada, T. Watanabe and K. Hashimoto, *J. Photochem. Photobiol., A*, 2003, **156**, 227–233.
35 T. Watanabe, A. Kitamura, E. Kojima, C. Nakayama, K. Hashimoto and A. Fujishima, *Photocatalytic Purification and Treatment of Water and Air*, Elsevier, New York, 1993, pp. 747–751.
36 J. L. Sagripanti, L. B. Routson and C. D. Lytle, *Appl. Environ. Microbiol.*, 1993, **59**, 4374–4376.
37 J. Bandara, C. P. K. Udawatta and C. S. K. Rajapakse, *Photochem. Photobiol. Sci.*, 2005, **4**, 857–861.
38 J. P. Yasomanee and J. Bandara, *Sol. Energy Mater. Sol. Cells*, 2008, **92**, 348–352.
39 T. Tatsuma, S. Saitoh, Y. Ohko and A. Fujishima, *Chem. Mater.*, 2001, **13**, 2838–2842.
40 T. Tatsuma, S. Saitoh, Y. Ohko and A. Fujishima, *Electrochemistry*, 2002, **70**, 460–462.
41 T. Tatsuma, S. Saitoh, P. Ngaotrakanwiwat, Y. Ohko and A. Fujishima, *Langmuir*, 2002, **18**, 7777–7779.
42 J. Li, Y. Liu, Z. J. Zhu, G. Z. Zhang, T. Zou, Z. J. Zou, S. P. Zhang, D. W. Zeng and C. S. Xie, *Sci. Rep.*, 2013, **3**, 2049.